Article

Cell Reports

Identification of Two Protein-Signaling States Delineating Transcriptionally Heterogeneous Human Medulloblastoma

Graphical Abstract

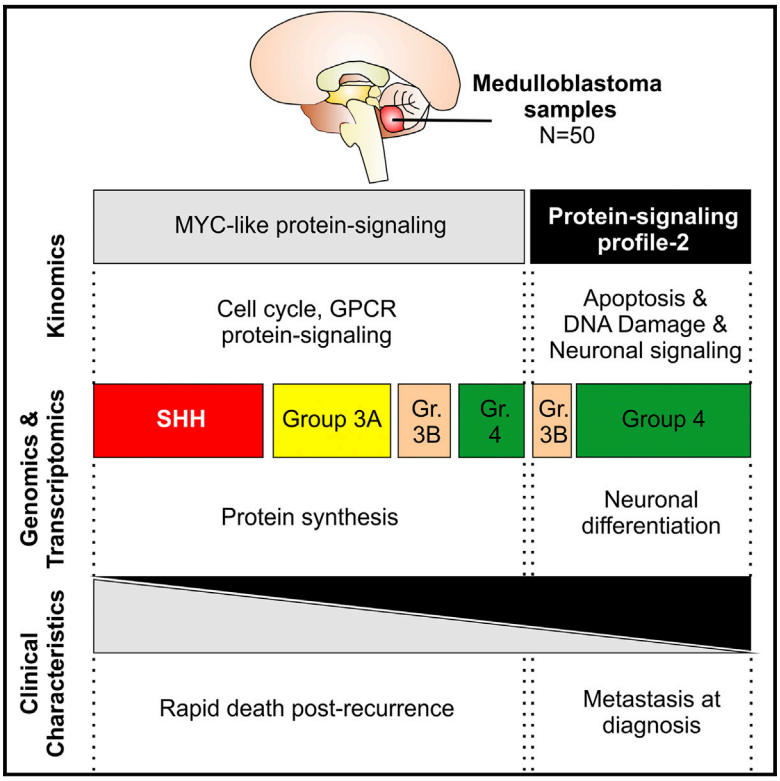

Highlights

- Two phosphoprotein-signaling profiles characterize human medulloblastoma
- Different transcriptional profiles can converge on one protein-signaling profile
- Targetable pathways are associated with the protein-signaling profiles
- MYC-like protein-signaling is associated with rapid death post-recurrence

Authors

Walderik W. Zomerman, Sabine L.A. Plasschaert, Siobhan Conroy, ..., Victor Guryev, Eveline S.J.M. de Bont, Sophia W.M. Bruggeman

Correspondence

s.w.m.bruggeman@umcg.nl

In Brief

Using peptide phosphorylation profiling, Zomerman et al. identify two medulloblastoma phosphoprotein-signaling profiles that have prognostic value and are potentially targetable. They find that these profiles extend across transcriptome-based subgroup borders. This suggests that diverse genetic information converges on common protein-signaling pathways and highlights protein-signaling as a unique information layer.

Zomerman et al., 2018, Cell Reports *22*, 3206–3216
March 20, 2018
https://doi.org/10.1016/j.celrep.2018.02.089

CellPress

OPEN ACCESS
CellPress

Cell Reports
Article

Identification of Two Protein-Signaling States Delineating Transcriptionally Heterogeneous Human Medulloblastoma

Walderik W. Zomerman,[1] Sabine L.A. Plasschaert,[1,9] Siobhan Conroy,[2] Frank J. Scherpen,[1] Tiny G.J. Meeuwsen-de Boer,[1] Harm J. Lourens,[1] Sergi Guerrero Llobet,[3] Marlinde J. Smit,[1] Lorian Slagter-Menkema,[2,4] Annika Seitz,[2] Corrie E.M. Gidding,[10] Esther Hulleman,[11] Pieter Wesseling,[9,12] Lisethe Meijer,[5] Leon C. van Kempen,[2,13] Anke van den Berg,[2] Daniël O. Warmerdam,[6] Frank A.E. Kruyt,[3] Floris Foijer,[6,7] Marcel A.T.M. van Vugt,[3] Wilfred F.A. den Dunnen,[2] Eelco W. Hoving,[8,9] Victor Guryev,[7] Eveline S.J.M. de Bont,[1,14] and Sophia W.M. Bruggeman[1,14,15,*]

[1]Departments of Pediatric Oncology and Hematology/Pediatrics, University of Groningen, University Medical Center Groningen, Hanzeplein 1, 9700 RB Groningen, the Netherlands
[2]Department of Pathology and Medical Biology, University of Groningen, University Medical Center Groningen, Hanzeplein 1, 9700 RB Groningen, the Netherlands
[3]Department of Medical Oncology, University of Groningen, University Medical Center Groningen, Hanzeplein 1, 9700 RB Groningen, the Netherlands
[4]Department of Otorhinolaryngology/Head and Neck Surgery, University of Groningen, University Medical Center Groningen, Hanzeplein 1, 9700 RB Groningen, the Netherlands
[5]Beatrix Children's Hospital, University of Groningen, University Medical Center Groningen, Hanzeplein 1, 9700 RB Groningen, the Netherlands
[6]iPSC CRISPR Center, University of Groningen, University Medical Center Groningen, Hanzeplein 1, 9700 RB Groningen, the Netherlands
[7]ERIBA, University of Groningen, University Medical Center Groningen, Hanzeplein 1, 9700 RB Groningen, the Netherlands
[8]Department of Neurosurgery, University of Groningen, University Medical Center Groningen, Hanzeplein 1, 9700 RB Groningen, the Netherlands
[9]Princess Máxima Center for Pediatric Oncology, Lundlaan 6, 3584 EA Utrecht, the Netherlands
[10]Department of Pediatric Oncology/Pediatrics, Radboud University Medical Center Nijmegen, Geert Groteplein Zuid 10, 6525 HB Nijmegen, the Netherlands
[11]Department of Pediatric Oncology/Hematology, Neuro-oncology Research Group, Cancer Center Amsterdam, VU University Medical Center Amsterdam, De Boelelaan 1117, 1081 HV Amsterdam, the Netherlands
[12]Department of Pathology, VU University Medical Center Amsterdam, De Boelelaan 1117, 1081 HV Amsterdam, the Netherlands
[13]Department of Pathology, McGill University, 3775 University Street, Montreal, QC H3A 2B4, Canada
[14]These authors contributed equally
[15]Lead Contact
*Correspondence: s.w.m.bruggeman@umcg.nl
https://doi.org/10.1016/j.celrep.2018.02.089

SUMMARY

The brain cancer medulloblastoma consists of different transcriptional subgroups. To characterize medulloblastoma at the phosphoprotein-signaling level, we performed high-throughput peptide phosphorylation profiling on a large cohort of SHH (Sonic Hedgehog), group 3, and group 4 medulloblastomas. We identified two major protein-signaling profiles. One profile was associated with rapid death post-recurrence and resembled MYC-like signaling for which MYC lesions are sufficient but not necessary. The second profile showed enrichment for DNA damage, as well as apoptotic and neuronal signaling. Integrative analysis demonstrated that heterogeneous transcriptional input converges on these protein-signaling profiles: all SHH and a subset of group 3 patients exhibited the MYC-like protein-signaling profile; the majority of the other group 3 subset and group 4 patients displayed the DNA damage/apoptotic/neuronal signaling profile. Functional analysis of enriched pathways highlighted cell-cycle progression and protein synthesis as therapeutic targets for MYC-like medulloblastoma.

INTRODUCTION

The overall cure rate for pediatric cancer has increased to approximately 80% over the past decades, yet there is an urgent need for further improvements (Pui et al., 2011). Current treatment strategies depend heavily on cytotoxic agents and radiotherapy, causing major side effects that have severe impact on the quality of life of survivors (Spiegler et al., 2004). Further, some pediatric malignancies remain difficult to target and have a dismal prognosis (Hassan et al., 2017). Recent efforts to map all pediatric cancer genomes have provided a tremendous wealth of information on the (epi)genetic background of the various pediatric cancer types (Downing et al., 2012). Not only is this knowledge highly valuable for classification and diagnostic purposes, but it also offers unprecedented potential for the development of new therapies and precision medicine.

Medulloblastoma, a malignant brain cancer that arises in the cerebellum, is one of the pediatric cancer types that has been the subject of intense investigation. Originally classified as a single disease, there is now consensus that, based on gene expression patterns, four main molecular medulloblastoma groups exist with different biological and clinical characteristics: WNT, SHH (Sonic Hedgehog), group 3, and group 4 (reviewed in Taylor et al., 2012). These groups can be further subdivided when combining different profiling strategies, such as gene expression analysis, genome-wide DNA methylation patterns, somatic copy number alterations and mutations, and clinical features, demonstrating considerable heterogeneity within medulloblastoma subgroups that is also recognized by the current World Health Organization (WHO) classification of central nervous system tumors (Cavalli et al., 2017; Louis et al., 2016; Northcott et al., 2017). Based on these studies, SHH medulloblastoma harboring TP53 mutations and MYC-amplified, metastasized group 3 medulloblastoma have the worst prognosis (Cavalli et al., 2017; Ramaswamy et al., 2016).

A less explored aspect in medulloblastoma research is the role of the tumor proteome, which turns (epi)genetic information into function (Anagnostopoulos et al., 2015; Staal et al., 2015). Part of the proteome constitutes the protein-signaling network that transduces and interprets signals required for faithful execution of most cellular processes (Aebersold and Mann, 2016). Disruptions in signaling routes implicated in cancer endow the cells with a growth advantage contributing to tumor growth (Hanahan and Weinberg, 2011). Various rational therapies that directly target proteins in these networks have been applied in patients, albeit with limited success (de Bono and Ashworth, 2010; Hanahan, 2014). Acquired resistance and rewiring of the protein-signaling networks toward parallel routes might be factors that contribute to the limited anti-tumor effect of these drugs. Therefore, it is essential to study protein signaling at the systems-biology level. This will deepen our understanding of protein networks, contribute to the development of novel therapies targeting all parallel signaling routes, and shed light on the channeling of (epi)genetic information into protein biology.

Here, we report the integration of transcriptional and genetic profiling with high-throughput peptide phosphorylation profiling as a measure for overall kinase activity, across a large cohort of untreated SHH, group 3, and group 4 medulloblastoma samples. Remarkably, medulloblastoma peptide phosphorylation profiling revealed two significant phosphoprotein-signaling profiles, while the cohort contained three different medulloblastoma subgroups based on gene expression. The first protein-signaling profile was reminiscent of signaling induced by the MYC oncoprotein that could occur in the absence of MYC aberrancies and was associated with rapid death post-recurrence. The second profile exhibited increased neuronal, apoptotic, and DNA-damage signaling. Functional analysis highlighted cell-cycle transition and protein synthesis as actionable targets in MYC-like medulloblastoma. Altogether, our data suggest that, despite heterogeneity at the genetic and transcriptional levels, downstream signaling in medulloblastoma ultimately converges on a limited number of potentially targetable signaling pathways, and they highlight that protein signaling constitutes a unique layer of information.

RESULTS

High-Throughput Peptide Phosphorylation Profiling Reveals Two Major Medulloblastoma Protein-Signaling Profiles

The main goal of our study was to gain insight into medulloblastoma protein signaling by performing high-throughput peptide phosphorylation profiling and subsequent integration with genetic and transcriptional profiling (Figure 1A). Untreated medulloblastoma samples were collected at diagnosis from three Dutch university medical centers. They were subjected to targeted exon sequencing of selected cancer-related genes (n = 49 out of 50 tumors), interphase fluorescence *in situ* hybridization (FISH; n = 42/50), transcriptional profiling (n = 48/50), and peptide phosphorylation profiling (n = 50/50) (Figure 1A). Clinical data were available for gender, patient age, and metastasis at diagnosis; treatment protocol; relapse; and survival (Table S1). Transcriptome analysis and unsupervised hierarchical clustering of differentially expressed genes showed that our patient cohort consisted of SHH (n = 13), group 3 (n = 16), and group 4 (n = 19) patients (Figures 1B and S1A). There were no WNT group tumors present in our cohort, likely due to their low frequency (Northcott et al., 2012). In agreement with previous findings, males were overrepresented in our cohort, and the transcriptomes of younger patients were generally assigned to SHH and group 3 (Figure 1C). Metastatic disease was most frequent in group 4 patients and associated with adverse outcome (Figures 1C, 1D, and S1B). There was no significant difference in survival between subgroups (Figure S1C).

We subjected protein lysates from all medulloblastoma samples to peptide phosphorylation profiling, using commercially available PTK (protein tyrosine kinase) and STK (serine/threonine kinase) PamChip arrays. These arrays measure the phosphorylation of synthetic peptides containing known substrate recognition sites for PTKs (n = 143 peptides) and STKs (n = 142 peptides) in a high-throughput fashion (Figure S2A). Unsupervised hierarchical clustering analysis using either the PTK or STK array identified the presence of two major protein-signaling profiles that consisted of peptides with relatively high phosphorylation intensity. These signaling profiles separated the tumors into protein-signaling clusters 1 and 2 that were largely overlapping between the STK and the PTK arrays (Figures 2A and S2B–S2D; Table S2). This was unexpected, given our earlier unpublished observations in a different type of brain cancer, glioblastoma, in which peptide phosphorylation profiling yielded multiple complex signaling profiles that did not correlate with subtype, survival, age, or gender (Figure S2E; Tables S1 and S2).

We noticed that there was a marked difference in the level of peptide phosphorylation intensities within STK protein-signaling cluster 1 samples. To address its biological relevance, based on branching of the clustering tree, we divided samples with the highest similarity in peptide phosphorylation intensities into subclusters 1A and 1B (Figures 2A, S2B, and S2C). Patients in subcluster 1A had a very low survival compared to the other patients, indicating the predictive value for this subcluster ($p = 0.0058$) (Figures 2B and S2F).

We then set out to further explore the biology of the protein-signaling profiles. Most peptides showing relatively high

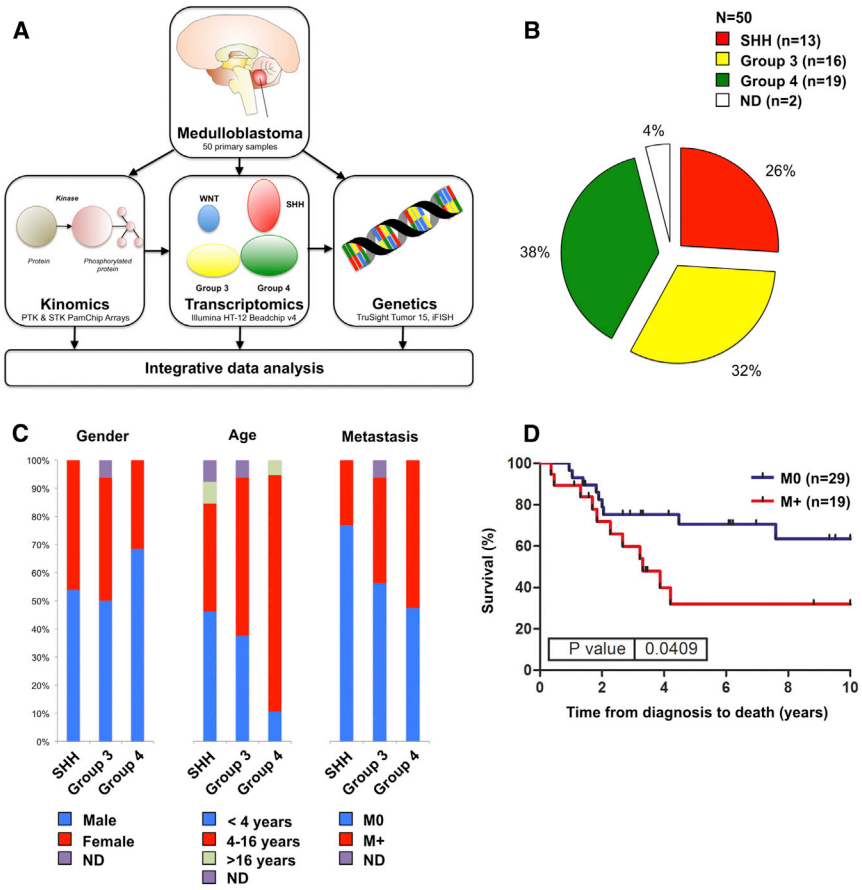

Figure 1. Overview of the Workflow and Medulloblastoma Patient Cohort Characteristics

(A) Overview of the workflow. N = 50 medulloblastoma samples from three Dutch university medical centers were included in the study. DNA (n = 49/50 tumors), nuclei (n = 42), mRNA (n = 48), and protein (n = 50) were isolated and analyzed for genetic alterations, gene expression, and peptide phosphorylation activity, respectively. Datasets were compared by integrative analysis.

(B) Pie chart showing the molecular subgrouping of N = 50 medulloblastoma patients (red indicates SHH, yellow indicates group 3, green indicates group 4, and white indicates ND [not determined]).

(C) Bar diagrams showing patient gender, age, and metastasis per molecular subgroup (M0, no metastasis; M+, metastasis at diagnosis).

(D) Kaplan-Meier curve showing the survival of medulloblastoma patients with (M+, red) and without (M0, blue) metastasis at diagnosis. The p values were determined using a log-rank (Mantel-Cox) test, and $p < 0.05$ was considered significant.

See also Figure S1 and Table S1.

phosphorylation levels in protein-signaling profile 1 have low phosphorylation of highly phosphorylated profile 2 peptides, and vice versa, which is suggestive of binary signaling states in medulloblastoma (Figure 2A). To identify the putative signaling pathways underlying these two states, we performed functional annotation of our signaling profiles using the Database for Annotation, Visualization and Integrated Discovery (DAVID) and visualized enriched processes using the Cytoscape Enrichment Map app (Figures 2C, S3, and S4; Table S2). While we did not identify clear, cluster-specific enriched pathways in the PTK protein-signaling profiles, we found that STK protein-signaling profile 1 displayed enrichment for cell-cycle transition and G-protein-coupled receptor signaling and that STK protein-signaling profile 2 was mostly enriched for DNA-damage response/p53 signaling, apoptotic signaling, response to external stimuli, and neuronal signaling (Figures 2C, S3, and S4). This is in line with the STKs constituting a larger fraction of the kinome and functioning in more diverse signaling pathways compared to PTKs. Further analyses, therefore, focused on STK protein signaling.

Medulloblastoma Protein-Signaling Clusters Partially Overlap with Molecular Subgroups

We next wanted to address the relationship between the previously established transcriptional medulloblastoma subgroups and our protein-signaling medulloblastoma clusters. Hereto, we first investigated how the transcriptionally defined medulloblastoma subgroups (i.e., SHH, group 3, and group 4) distributed across the protein-signaling clusters. We divided group 3 tumors into subgroups 3A and 3B due to marked transcriptional heterogeneity and in agreement with earlier findings describing overlap in transcriptomes between subsets of group 3 and group 4 medulloblastoma (Figure S1A) (Kool et al., 2008; Taylor et al., 2012). We found that SHH tumors were exclusively in protein-signaling cluster 1. Group 3 tumors were enriched in cluster 1, whereas group 4 tumors were predominantly found in protein-signaling cluster 2 (Figure 3A). Fifty-one peptides correlated significantly with the SHH group, 4 peptides correlated with group 3A, 1 peptide correlated with group 3B, and 76 peptides correlated with group 4 (false discovery rate [FDR] < 0.05; Table S2). We also re-plotted the data to visualize the protein-signaling profiles per transcriptional subgroup (Figure 3B). These data suggest that gene-expression-based tumor profiling largely correlates with protein-signaling profiling. However, there is a subset of group 3 and group 4 tumors that localizes to the opposite protein-signaling cluster. To investigate whether subtle differences in gene expression could be underlying this, we plotted medulloblastoma transcriptional profiles against the protein-signaling clusters (Figure 3C). Group 3B, which shares characteristics with group 4, contained all group-3 tumors exhibiting protein-signaling profile 2, suggesting that group-4-like gene expression contributes to this protein-signaling profile. Altogether, these results demonstrate that gene expression strongly, though not fully, correlates with protein signaling and, importantly, that different transcriptional profiles channel into the same protein-signaling pathway.

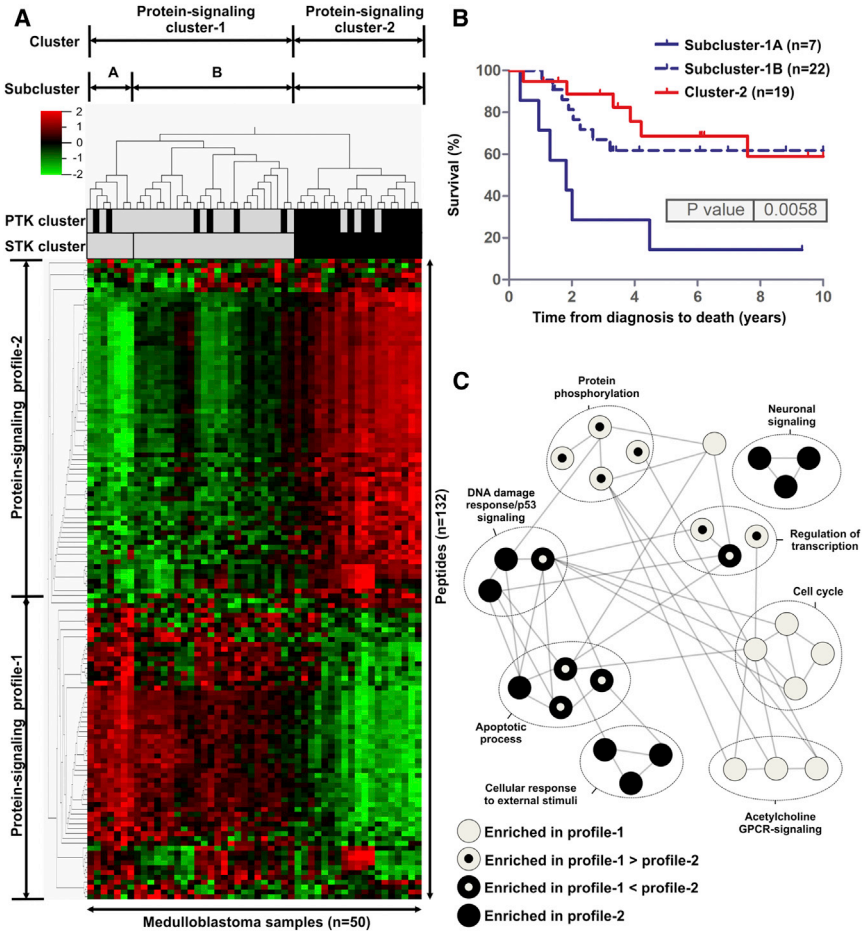

Figure 2. High-Throughput Peptide Phosphorylation Profiling Reveals Two Medulloblastoma Protein-Signaling Profiles with Specific Enriched Biological Processes

(A) Heatmap showing the unsupervised hierarchical clustering of normalized differential peptide phosphorylation intensities of n = 142 different synthetic peptides with serine/threonine kinase (STK) recognition sites across N = 50 medulloblastoma samples. Peptides clustered into two profiles termed protein-signaling profile 1 and protein-signaling profile 2. Patients clustered into two main clusters, termed protein-signaling cluster 1 (gray) and cluster 2 (black). Patient clusters were further subdivided into subclusters 1A, 1B, and 2. PTK-based patient clusters were overlaid.

(B) Kaplan-Meier curve showing survival of medulloblastoma patients in the different STK protein-signaling (sub)clusters. The p values were determined using a log-rank (Mantel-Cox) test, and $p < 0.05$ was considered significant.

(C) Enrichment map representing biological processes enriched in the different protein-signaling profiles. Each node represents a biological process grouped and labeled by biological theme. Biological processes connected by edges have proteins in common. Enriched biological processes were determined with the Database of Annotation, Visualization and Integrated Discovery (DAVID), v.6.8 (Benjamini-corrected q = 0.1, p = 0.01) and visualized with the Enrichment Map app in Cytoscape.

See also Figures S2, S3, and S4 and Table S2.

MYC-like Signaling Defines the Main Medulloblastoma Protein-Signaling Profile and Is Associated with Rapid Death Post-recurrence

After identifying two protein-signaling profiles in our medulloblastoma cohort, we set out to unravel the molecular mechanism imposing these profiles. We hypothesized that potent (proto)oncogenes, inducing replication stress, or lost tumor suppressor genes are potential candidates. Therefore, we set out by analyzing the medulloblastoma transcriptome data for expression levels of the *MYC* oncogenes and the *TP53* tumor suppressor gene, which have been postulated as important players in medulloblastoma (Figure S5A) (Hill et al., 2015; Kawauchi et al., 2012; Pei et al., 2012; Roussel and Robinson, 2013). We observed that a number of tumors in protein-signaling cluster 1 displayed relatively high mRNA expression of MYC (mainly group 3 tumors), or MYCN ($p < 0.001$) (mainly SHH tumors), although this was not true for all tumors. Group 4 tumors showed relatively low MYC expression levels. MYCL did not show differential gene expression. Intriguingly, TP53 expression was significantly higher in a subset of protein-signaling cluster 1 tumors but low across cluster 2 ($p < 0.001$). These observations suggest that *MYC* and *TP53* could be involved in dictating the protein-signaling profiles.

To model oncogene-induced replication stress and tumor suppressor function, we made use of an *in vitro* system of non-cancerous, diploid human cells (hTERT immortalized retinal pigmented epithelial cells, hereinafter called RPE-1). We generated RPE-1 cell lines overexpressing MYC, MYCN, CCNE1 (CYCLIN E1), or CDC25A, lesions known to provoke replication stress (Figures S5B and S5C). These RPE-1 cell lines were either *TP53* wild-type, *TP53* mutant (insensitive to MDM2 inhibitor Nutlin-3), or *TP53* null (Figures S5C and S5D). Cell lysates from these models were subjected to peptide phosphorylation profiling on the STK array and analyzed in a manner similar to that for the medulloblastoma patient samples (Figures 4A and S5E; Table S2). The specificity of this model was validated by provoking differential TP53 responses in wild-type or TP53 null RPE-1 cells using either Nutlin-3 or irradiation, which resulted in different protein-signaling profiles for each condition (Figures S5F and S5G; Table S2). Unsupervised hierarchical clustering showed that overexpression of both MYC and MYCN induces a strong shift in the peptide phosphorylation profile as compared to empty vector control cells, which was even more apparent upon loss of p53 function (Figure 4A). Surprisingly, loss of p53 activity alone yielded a reciprocal profile reminiscent of control cells, suggesting that this profile resembles baseline protein signaling that is, at least, partially p53

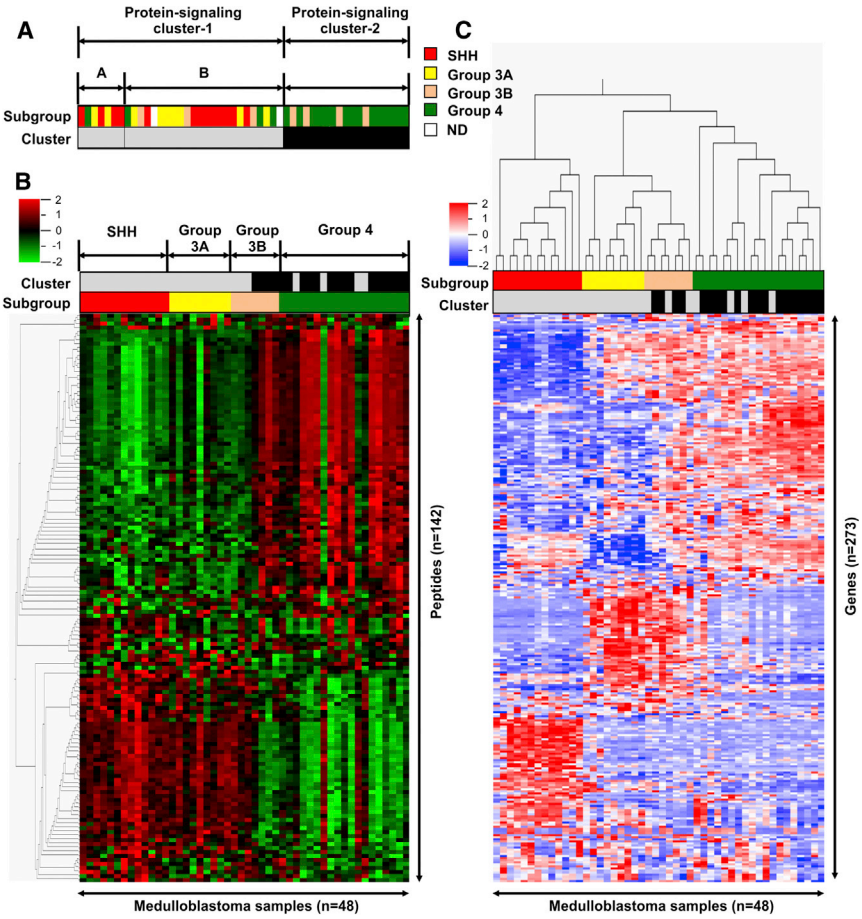

Figure 3. Medulloblastoma Protein-Signaling Clusters Partially Overlap with Molecular Subgroups

(A) Overlap of transcriptional subgroups and protein-signaling clusters (gray indicates cluster-1, black indicates cluster-2, red indicates SHH, yellow indicates group 3A, orange indicates group 3B, and green indicates group 4).

(B) Heatmap showing the supervised hierarchical clustering of STK peptide phosphorylation array profiling based on molecular subgrouping.

(C) Heatmap showing unsupervised hierarchical clustering of gene expression intensities of medulloblastoma samples overlaid with the STK protein-signaling clusters.

See also Table S2.

independent. CDC25A and CCNE1 overexpression also induced profiles similar to those of control, indicating that the *MYC* oncogenes are unique in their response. However, when p53 function is impaired, CCNE1 cells partially shifted toward the MYC profile, implying that genetic lesions can collaborate to mimic MYC-induced signaling (Figure 4A).

To test our hypothesis that (onco)genes such as *MYC* and *TP53* could be sufficiently powerful to impose a medulloblastoma protein-signaling profile upon a tumor, we took the peptides showing highest differences in phosphorylation intensity across all MYC and MYCN RPE-1 samples compared to control and established the degree of overlap with the relatively high intensity peptides of the medulloblastoma protein-signaling profiles (Figure 4B; Table S2). This analysis yielded a 94% overlap with protein-signaling profile 1 and basically no overlap with profile 2. Comparison with the highest intensity peptides from the p53 activation experiment showed only a modest overlap (72%) with signaling profile 2 (Figures 4B and S5G; Table S2). Hence, we renamed medulloblastoma protein-signaling profile-1 "MYC-like" and concluded that, whereas TP53 loss might contribute to this profile, p53 activation status cannot explain either of the protein-signaling profiles. Interestingly, it has recently been shown that gain of *MYC* and loss of *TP53* function upon recurrence is common and predictive of rapid death due to progressive disease in medulloblastoma (Hill et al., 2015). When we explored time to death post-recurrence in our cohort, we observed that patients with a MYC-like signaling profile succumbed significantly faster than patients with the opposite signaling profile ($p = 0.0151$) (Figure 4C). This indicates that protein-signaling profiling can predict clinically aggressive disease after relapse already at diagnosis.

MYC Overexpression or Amplification Is Dispensable for the MYC-like Medulloblastoma Protein-Signaling Profile

We had already observed that MYC, MYCN, and TP53 expression was elevated in some, but not all, tumors (Figure S5A). We then wanted to address whether genomic alterations, such as *MYC* amplifications or *TP53* mutations, could underlie the two medulloblastoma protein-signaling profiles. Interphase FISH was used to detect amplifications of the *MYC* and *MYCN* gene loci (Figures 5 and S6A). Only 2 out of 42 tumors tested showed amplification of *MYC*. One was a group 3 medulloblastoma belonging to MYC-like protein-signaling cluster 1, which had *MYC* amplifications in a substantial number of tumor cells. The other tumor was a group 4 medulloblastoma of protein-signaling cluster 2 with a minor *MYC*-amplified subclone. None of the 42 tested tumors had *MYCN* amplifications.

Subsequently, we performed targeted exon sequencing to identify *TP53* mutations (Figure 5; Table S4). We hypothesized that the increased TP53 mRNA expression levels in the MYC-like tumor cluster are related to mutations in the *TP53* gene, endowing p53 with pro-oncogenic activity (Levine, 1997). In agreement, we found that the 3 tumors with *TP53* point mutations were in the MYC-like protein-signaling cluster. Intriguingly, one of these patients also had a *MYC* amplification and belonged to subcluster 1A, exhibiting poor overall survival.

Lastly, we attempted to call copy number aberrations based on transcriptome data, which provides a rough estimate of tumor aneuploidy (Figures 5 and S6B). We could detect a number

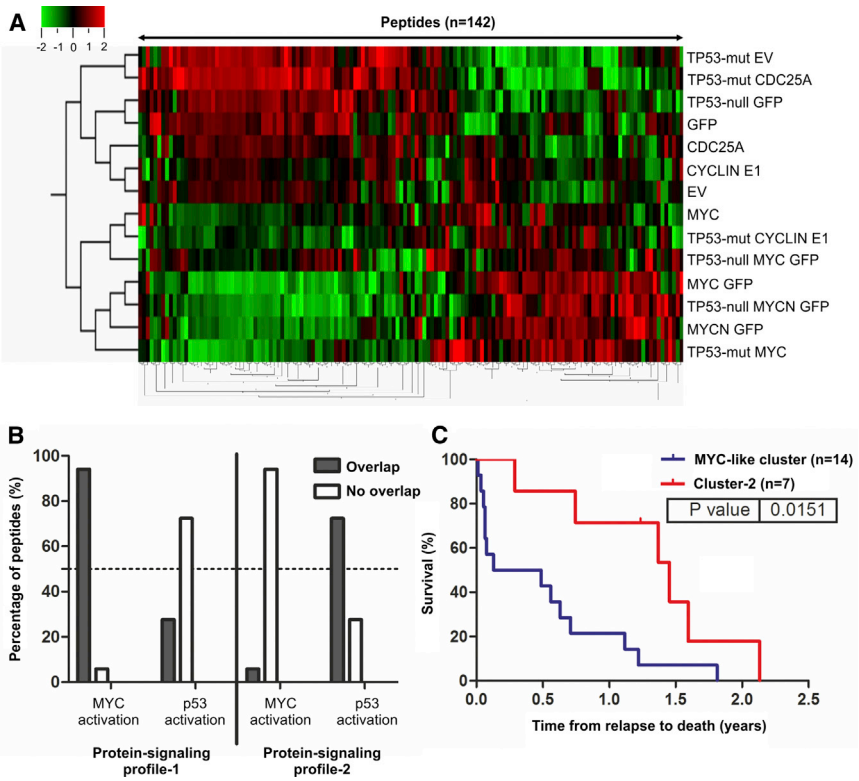

Figure 4. MYC-like Signaling Defines the Main Medulloblastoma Protein-Signaling Profile and Is Associated with Rapid Death Post-recurrence

(A) Heatmap showing the unsupervised hierarchical clustering of STK peptide phosphorylation intensities in RPE-1 TP53 wild-type and RPE-1 TP53 mutant/TP53 null cells, with or without MYC, MYCN, CYCLIN E1, and CDC25A overexpression. EV, empty vector; TP53-mut, TP53 mutant.

(B) Bar plot showing the overlap between peptides up- or downregulated in medulloblastoma protein-signaling profiles and peptides up- or downregulated in MYC activation or p53 activation profiles.

(C) Kaplan-Meier curve showing the time from relapse to death of medulloblastoma patients in the MYC-like signaling cluster versus signaling cluster 2. The p values were determined using a log-rank (Mantel-Cox) test, and $p < 0.05$ was considered significant.

See also Figure S5 and Table S2.

of chromosome arm gains and losses previously associated with medulloblastoma, such as on chromosomes 1, 7, 8, 9, 10, 16, and 18 (Northcott et al., 2012). Between the two protein-signaling clusters, the only differential copy number alterations found were on chromosomes 17 and 21. Of note, chromosome 17 abnormalities are frequently attributed to isochromosome 17q/i(17q), which is associated with (partial) loss of *TP53* expression and enriched in our protein-signaling cluster 2 (Bien-Willner and Mitra, 2014). In conclusion, genetic alterations are highly associated with changes in mRNA expression as expected. Together, they explain the protein-signaling profiles of most, but not all, of the tumors in our cohort, suggesting that protein signaling constitutes a discrete informational layer.

Protein-Signaling Profiling Uncovers Therapeutic Targets for MYC-like Medulloblastoma

Functional annotation of the protein-signaling profiles had identified enriched pathways for each profile (Figure 2C). We reasoned that these pathways could be exploited as targets for treatment, as they likely fulfill key roles in tumor protein signaling. Two processes enriched in signaling profile 2 were apoptotic signaling and DNA damage/p53-mediated response. Considering the relatively low TP53 mRNA expression levels (Figure S5A), absence of *TP53* point mutations, and high incidence of i(17q) in this group (Figure 5), we hypothesized that increasing p53 activity could have an anti-tumorigenic effect in these patients (Künkele et al., 2012). However, all human medulloblastoma cell lines that we analyzed on the STK array exhibited a (partial) MYC-like profile, precluding testing of this hypothesis (Figure S7). Therefore, we focused on processes enriched in the MYC-like signaling profile and selected cell-cycle progression as a putative actionable target (Figure 2C). We reasoned that this process reflects the replication stress that accompanies MYC-like signaling. It had been demonstrated previously that oncogene-induced replication stress sensitizes cells for the suppression of proteins involved in the G2/M transition, which prompted us to test the drug sensitivity of medulloblastoma cell lines for inhibitors of G2/M components ATR and WEE1 (Harris et al., 2014; Schoppy et al., 2012). We observed that all cell lines were sensitive to the lead compounds MK-1775 (WEE1 inhibitor) and VE-822 (ATR inhibitor) (Figure 6A). Especially the medulloblastoma cell lines with *MYC* amplifications (MED8A and HD-MB03) showed high sensitivity to ATR inhibition.

Lastly, we wanted to address whether the detection of targetable pathways based on protein-signaling profiling is restricted to the level of proteins or whether they are also discernable at the level of the transcriptome. Hereto, we performed supervised hierarchical clustering of medulloblastoma samples based on protein-signaling clusters and selected the genes that were significantly up- or downregulated ($p = 5E^{-5}$) (Figure 6B; Table S5). The regulated genes, which did not show overlap with previously published MYC signatures, clustered into two major groups, each containing one enriched biological theme: protein synthesis-related processes in MYC-like cluster tumors and neuronal differentiation processes in signaling cluster 2 tumors (Figure 6C; Table S5) (Coller et al., 2000; Jung et al., 2017; Valentijn et al., 2012). Both themes have previously been recognized as enriched in two or more of the medulloblastoma transcriptional subgroups; however, they have not been singled out as uniquely correlated with shared protein-signaling profiles (Kool et al., 2008). Protein synthesis is a process tightly

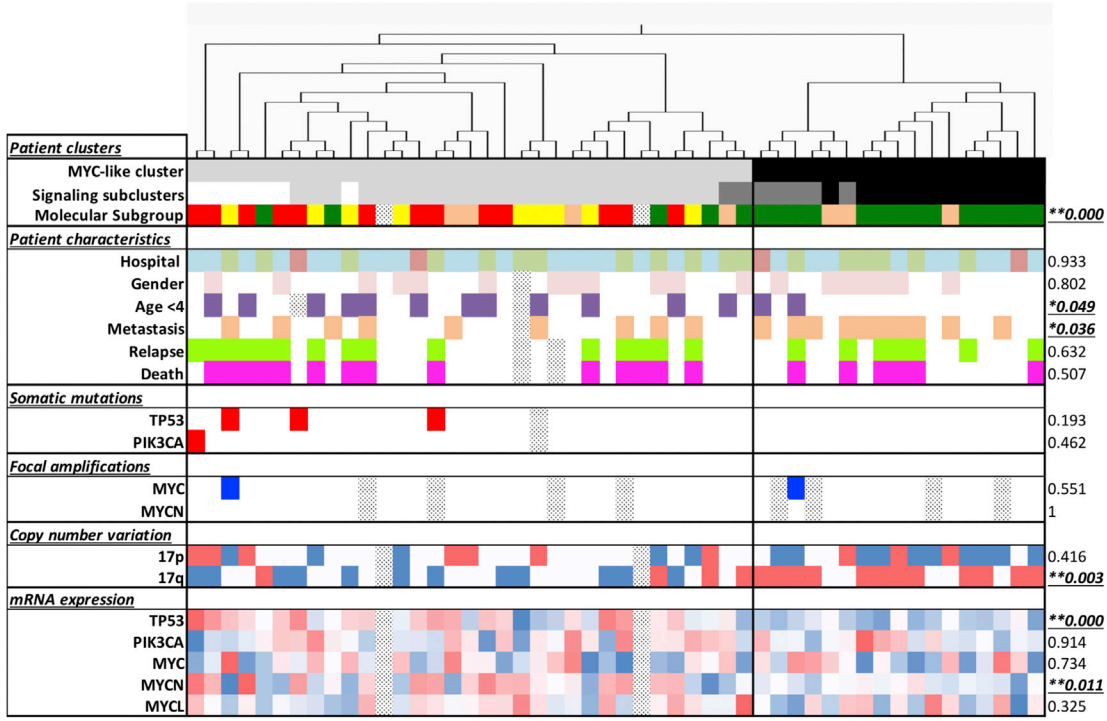

Figure 5. Summary of Medulloblastoma Patient Clusters, Characteristics, Somatic Mutations, Focal Amplifications, Copy Number Variations, and mRNA Expression Levels Grouped by the MYC-like Protein-Signaling Cluster

Rows are described from top to bottom. Distribution of protein-signaling clusters (gray indicates MYC-like cluster, and black indicates signaling cluster 2). Signaling subclusters (white indicates cluster 1A, gray indicates cluster 1B, and black indicates cluster 2). Molecular subgroups (red indicates SHH, yellow indicates group 3A, orange indicates group 3B, green indicates group 4, and white indicates ND [non-determined]). Patient characteristics (medical center: blue indicates UMCG, light green indicates RUMC, and light red indicates VUMC; gender: white indicates male, and pink indicates female; age: purple indicates <4 years, and white indicates ≥4 years; metastasis: white indicates M0, and orange indicates M+; relapse: green indicates yes, and white indicates no; death: violet indicates yes, and white indicates no). Somatic mutations (red indicates mutation, and white indicates no mutation). Focal amplifications (blue indicates amplified. and white indicates non-amplified). Large copy number variations (red indicates gain, and blue indicates loss) deduced from gene expression levels. mRNA expression levels (red indicates high expression, and blue indicates low expression). Missing data are indicated by a black dotted fill. The p values were determined using a chi-square test or Student's t test, and $p < 0.05$ was considered significant. *$p < 0.05$; **Benjamini-corrected $q < 0.05$.
See also Figure S6 and Tables S2 and S4.

associated with MYC function and has been proposed as an anti-cancer target (van Riggelen et al., 2010; Truitt and Ruggero, 2016). Therefore, we performed a proof-of-principle experiment to test whether our medulloblastoma cell lines were sensitive to protein synthesis inhibition. As anticipated, all medulloblastoma cell lines were sensitive to the protein synthesis inhibitor Brusatol; however, MYC-amplified cells were roughly eight times more sensitive (lethal concentration [LC50], mean ± SEM: 4.25 nM ± 2.56 nM) than non-MYC amplified cells (LC50, mean ± SEM: 32.78 nM ± 4.50 nM) (Figure 6D).

DISCUSSION

In this study, we have assessed kinome-wide phosphoprotein-signaling across a cohort of primary human medulloblastoma. We identified two major protein-signaling profiles, which was unexpected, given the presence of three molecular medulloblastoma subgroups, i.e., SHH, group 3, and group 4. These findings suggest that different gene expression profiles can coalesce into common signaling profiles and that protein signaling is a discrete layer of information that is not directly inferable from tumor genetics.

Two Protein-Signaling Profiles Delineate Human Medulloblastoma

It is important to understand the pathways used by tumors to relay signals, as this will aid the development of targeted therapies. However, the study of proteins at the systems level is challenging, due to the limited detection depths of current techniques, which is particularly relevant for the vast post-translationally modified proteome (Aebersold and Mann, 2016; Akbani et al., 2014; Sharma et al., 2014). The approach we have taken is not exhaustive, yet it allows for assessing the potential activity of a large part of the kinome, thereby yielding the two broad protein-signaling profiles. Future advancements in the proteomics field will elucidate whether additional medulloblastoma protein-signaling subtypes exist, similar to the diversification of molecular subtypes that followed from advanced (epi)genetic profiling (Cavalli et al., 2017; Northcott et al., 2017).

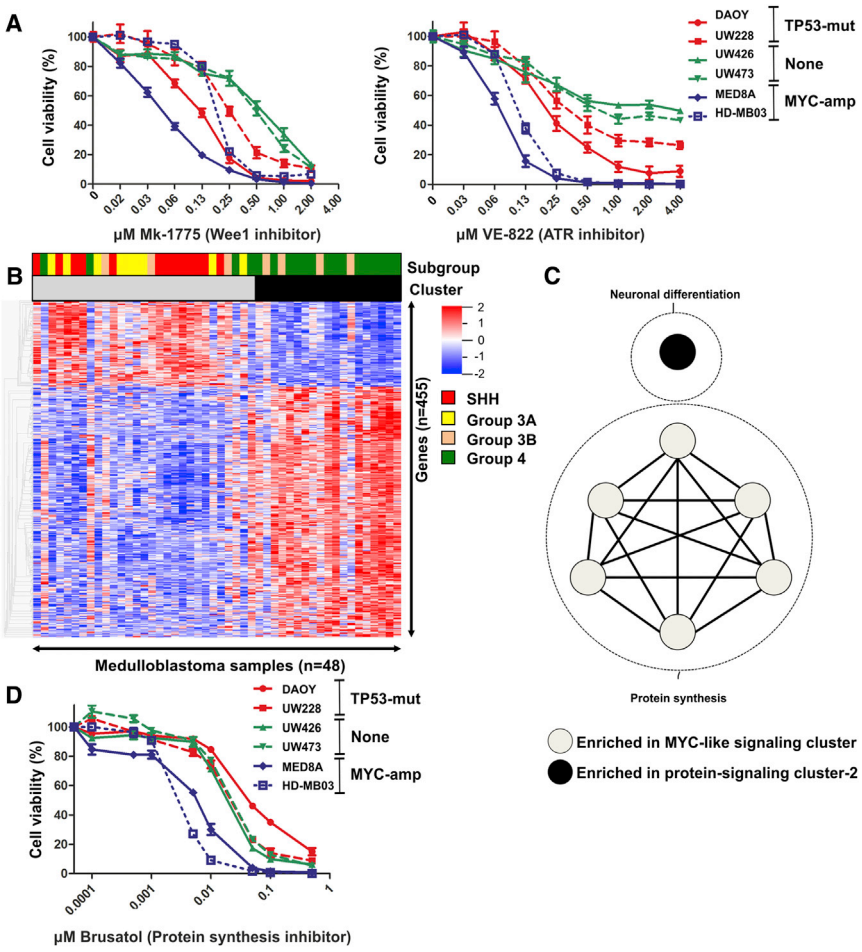

Figure 6. Protein-Signaling Profiling Uncovers Therapeutic Targets for MYC-like Medulloblastoma

(A) Cell viability assays showing the effects of WEE1 (MK-1775) and ATR inhibition (VE-822) on the viability of medulloblastoma cell lines with different TP53 and MYC genetic backgrounds. Data points represent mean ± SEM. TP53-mut, cell lines with *TP53* mutations; MYC-amp, cell lines with MYC amplifications.

(B) Heatmap showing supervised hierarchical clustering of significantly up- or downregulated genes (Student's t test; $p < 5E^{-5}$) in medulloblastoma samples belonging to the MYC-like protein-signaling cluster (gray) versus samples belonging to protein-signaling cluster 2 (black). The molecular subgroup assigned to each sample is marked on top (red indicates SHH, yellow indicates group 3A, orange indicates group 3B, green indicates group 4, and white indicates ND [not determined]).

(C) Enrichment map representing biological processes enriched in profile-specific upregulated genes (Student's t test; $p < 5E^{-5}$) for the MYC-like protein-signaling profile (gray nodes) and protein-signaling profile 2 (black node). Each node represents a biological process grouped and labeled by biological theme. Biological processes connected by edges have genes in common. Enriched biological processes were determined with the Database of Annotation, Visualization and Integrated Discovery (DAVID), v.6.8 (Benjamini-corrected q = 0.1, p = 0.01) and visualized with the Enrichment Map app in Cytoscape.

(D) Cell viability assays showing the effects of the protein synthesis inhibitor Brusatol on the viability of medulloblastoma cell lines with different *TP53* and *MYC* genetic backgrounds. Data points represent mean ± SEM.

See also Figure S7 and Table S5.

A Subset of Medulloblastoma Exhibits a MYC-like Signaling Profile for which MYC Aberrations Are Sufficient but Not Necessary

The most frequent protein-signaling profile in the cohort was highly reminiscent of MYC-induced protein signaling in the RPE-1 cell-culture model and was, therefore, termed "MYC-like." MYC signatures have been described in human cancer, but based on gene expression and genetic lesions and not on protein signaling, explaining a lack of overlap with genes in our MYC-like cluster (Coller et al., 2000; Jung et al., 2017; Valentijn et al., 2012). Genetic and transcriptional analyses showed that, for a number of these tumors, amplification or elevated expression of the *MYC* family oncogenes could account for the MYC-like profile, though there were also tumors that did not show any MYC-related abnormalities, indicating that the MYC-like signaling profile is not dependent on MYC lesions. From this, we conclude that MYC-like signaling represents a cell-biological state that is defined by MYC signaling characteristics but that can be relayed by other lesions that, alone or in combination, confer a MYC-like state upon the tumor. In line, in our *in vitro* model system, we observed that overexpression of CYCLIN E1 could also evoke a MYC-like profile, but only in combination with a *TP53* alteration. Likewise, the medulloblastoma sample harboring a *PIK3CA* point mutation could depend on phosphatidylinositol 3-kinase (PI3K) signaling for imposing the MYC-like protein-signaling profile. The idea that different combinations of genetic lesions or expression patterns channel into one protein-signaling profile reconciles our observation that different medulloblastoma transcriptomes exist within a protein-signaling cluster. For future studies, it would be interesting to include WNT medulloblastomas, which are somewhat paradoxically characterized by high MYC expression while having a favorable prognosis (Roussel and Robinson, 2013).

MYC-like Signaling and Protein Synthesis versus Apoptotic and Neuronal Signaling: Two Sides of the Same Coin?

A remaining question is the mechanism behind the second protein-signaling profile that dominates group 4 medulloblastoma. We found that this profile is associated with apoptotic signaling, DNA-damage signaling, and neuronal signaling and differentiation and that it shares features with protein signaling in untransformed, cycling cells. The unequivocally low TP53 mRNA expression coinciding with a high incidence of i(17q) implies a

reduction, but not absence, of functional p53 protein. Therefore, we hypothesize that part of the profile and oncogenic capacity of these tumors lies in a partially impaired response of the TP53 tumor suppressor pathway, hampering apoptosis-mediated removal of excessive or precociously differentiated neurons. Enhancing the remaining p53 function, such as by Nutlin-3 treatment, could be beneficial for these patients.

It should be noted, though, that in the MYC-like cluster, there are also patients with low TP53 expression or i(17q). How can we explain that they show the opposite, MYC-like protein-signaling profile? As an answer to this question, we propose that the MYC-like profile represents a different side of the same coin. Depending on levels and context, MYC controls stem cell properties and differentiation and could, therefore, counteract neuronal differentiation while simultaneously inducing protein synthesis, giving rise to the MYC-like signaling profile (Akita et al., 2014; Dang, 2012; Fagnocchi and Zippo, 2017; Kim et al., 2010; Leon et al., 2009). This idea also raises the interesting point that the MYC-like profile is dominant over the other profile and acts as a switch. This is supported by our data in RPE-1 cells, in which MYC overexpression induces a MYC-like signaling state, regardless of *TP53* status. If true, we expect to find evidence of medulloblastoma samples switching during tumor progression. Intriguingly, there is one group 4 patient in protein-signaling cluster 2 who is positioned at the border between the two clusters. At diagnosis, this tumor contained a minor clone exhibiting MYC amplification. It is conceivable that this tumor has adopted the MYC-like signaling profile upon further clonal selection of the MYC-amplified cells, which might then have contributed to the rapid death of this patient.

To definitively prove this point, primary and corresponding relapse samples should be analyzed. The few studies on rare medulloblastoma relapse material have shown that, while molecular subgroups remain stable during progression, histological and mutational characteristics change upon recurrence, and, hence, protein-signaling profiles might also switch (Hill et al., 2015; Morrissy et al., 2016; Ramaswamy et al., 2013; Wang et al., 2015). Moreover, *TP53* pathway defects and *MYC* gene family amplifications were the only lesions significantly associated with relapse and subsequent time to death in all medulloblastoma subgroups, which is in line with MYC and TP53 mediating the protein-signaling profiles (Hill et al., 2015).

The MYC-like Signaling Profile Is Associated with Rapid Death upon Relapse but May Be Targetable

While the overall survival between the two protein-signaling clusters is similar, patients with a MYC-like profile fare worse if the disease recurs. Possibly, MYC-like signaling endows the tumor cells with cancer stem cell properties, including increased resistance to therapy (Cojoc et al., 2015; Galardi et al., 2016; Wang et al., 2013). Alternatively, continuous replication stress induces genomic instability, increasing the mutational burden and clonal heterogeneity. Hence, it seems worthwhile to target the MYC-like properties of these tumors at diagnosis, either by direct MYC inhibition or by interference with downstream processes like cell-cycle transition and protein synthesis, which we found to be enriched in MYC-like tumors (van Riggelen et al., 2010; Roussel and Robinson, 2013; Soucek et al., 2013; Truitt and Ruggero, 2016; Whitfield et al., 2017). Using medulloblastoma cell lines to model MYC-like medulloblastoma, we performed proof-of-concept experiments demonstrating that the targeting of cell-cycle transition or protein synthesis can attenuate MYC-like medulloblastoma growth *in vitro*. Since we used cell lines and lead compounds for our experiments, further clinical testing will determine whether such strategies are also applicable in patients.

Altogether, we have demonstrated that two major protein-signaling profiles are present across a cohort of primary medulloblastoma samples that are genetically and transcriptionally heterogeneous. This indicates that (epi)genetic information converges on a limited number of protein-signaling pathways, which might represent key actionable targets for medulloblastoma treatment.

EXPERIMENTAL PROCEDURES

Patient Samples

Tumor tissue was obtained from N = 50 untreated primary medulloblastomas at diagnosis from three Dutch university medical centers (University Medical Center Groningen, Radboud University Medical Center Nijmegen, and VU University Medical Center Amsterdam) by surgical resection. The tissue of N = 30 primary glioblastomas was obtained from the University Medical Center Groningen by surgical resection. Immediately following surgical resection, tissue samples were snap frozen in liquid nitrogen and stored at −80°C until further processing. Patient information on gender, age at diagnosis, and subtype is presented in Table S1. Tumor material was histologically evaluated by an experienced neuropathologist and examined for tumor content. Samples were excluded from analysis when tumor content was below 70%. Informed consent and local medical ethical committee approval was granted for use of the patient material.

Cell Lines, Cell Culture, and Pharmacologic Inhibition

Human medulloblastoma cell lines RES256, UW402, UW426, and UW473 were kindly provided by Dr. Michael Bobola. UW228, ONS76, MED8A, and HD-MB03 were kindly provided by Dr. Till Milde. DAOY, D283MED, and hTERT-immortalized retinal pigmented epithelium cell line (RPE-1) were purchased at the American Type Culture Collection (ATCC). DAOY, RES256, ONS76, UW228, UW402, UW426, UW473, RPE-1, and MED8A cells were cultured in DMEM growth medium. The human medulloblastoma cell line D283MED was cultured in Eagle's minimal essential medium (EMEM) growth medium, and HD-MB03 was cultured in RPMI growth medium. All cell lines were maintained at 37°C in a humidified atmosphere of 5% CO_2. All growth media were supplemented with 10% fetal calf serum (GIBCO), 100 U/mL penicillin, and 100 μg/mL streptomycin (GIBCO). Details regarding the origin of human cell lines used in this paper have been provided in Table S6. RPE-1 cells were treated with 6 Gy irradiation, MDM2 inhibitor Nutlin-3 (Selleck Chemicals, S1061) (0–32 μM), etoposide (10 μM), and cisplatin (10 μM); and human medulloblastoma cell lines were treated with WEE1 inhibitor MK-1775 (Selleck Chemicals, S1525) (0–2 μM), ATR inhibitor VE-822 (Selleck Chemicals, S7102) (0–4 μM), or protein synthesis inhibitor Brusatol (Sigma-Aldrich, SML1868) (0–0.5 μM).

Gene Expression Profiling and Tumor Subgrouping

To generate gene expression profiles, total RNA was hybridized to the Human HT-12 Expression BeadChip system, v.4 (Illumina) according to the manufacturer's protocol. Gene expression data were extracted and quantile normalized using custom Perl scripts. To determine the molecular subgrouping of the medulloblastoma samples, unsupervised hierarchical clustering analysis was performed using a variance filter of 0.45 (σ/σ_{max}) in Qlucore Omics Explorer (v.3.2). For glioblastoma tumors, subgroups were determined by the presence of the $IDH1^{R132H}$ mutation (proneural $IDH1^{mut}$), EGFR amplification combined with EGFR exon 2–7 deletion (EGFRVIII positive, classical-like), or high expression of mesenchymal markers (mesenchymal-like) (Conroy et al., 2014).

Peptide Phosphorylation Profiling

Tyrosine and serine/threonine peptide phosphorylation profiles were determined using the commercially available PamChip PTK or STK microarray system (PamGene). These microarrays consist of n = 143 or n = 142 unique peptide sequences, respectively. Each peptide represents a 13- to 15-amino-acid sequence corresponding to a phosphorylation site, which serves as a kinase substrate. Together, these peptides are predicted to cover the activity of around 65% of the human kinome (13% and 52% for the PTK and STK PamChip arrays, respectively). The experiment was repeated 3 times for each medulloblastoma tissue sample. For human cell lines, the experiment was repeated 1–3 times.

Identification of Somatic Mutations

The mutation status of *TP53* was analyzed by next-generation sequencing using the Illumina TruSight Tumor (TST) 15 assay (Illumina) at the Molecular Pathology Center of the Jewish General Hospital (Montreal, QC, Canada). The CAP-compliant clinically validated TST15 assay was performed as per the supplier's instructions with 10 ng DNA input. Libraries were sequenced on the MiSeq Reagent Kit with a v3 flow cell (Illumina). Data were analyzed with a clinically validated pipeline (NextGENe, SoftGenetics), and variants were annotated in Geneticist Assistant (SoftGenetics). The International Agency for Research on Cancer (IARC) TP53 database, v.R18, was consulted for the molecular interpretation of *TP53* variants (http://www.p53.iarc.fr).

Cell Viability Assays

To examine the effect of cell cycle or protein synthesis inhibition, WST-1 colorimetric viability assays (Roche) were used, following the manufacturer's protocol guidelines. Human medulloblastoma cells were seeded in sextuple at a density of 10,000 per well in a 96-well plate format. After attachment, cells were treated with appropriate inhibitor concentrations. All inhibitors were dissolved in DMSO and DMSO concentrations were kept constant between the different conditions. Optical densities were measured using a microplate reader (Bio-Rad) at 450 nm. Optical densities of wells containing cells were subtracted by the intensity of a blank control well and normalized relative to the optical densities of wells containing control-treated cells (100%).

Statistical Analysis

Differences in the expression of individual genes between protein-signaling profiles or across molecular subgroups were compared using the two-sample Student's t test, assuming equal variances. Patient characteristics of patients belonging to the MYC-like protein-signaling cluster or protein-signaling cluster 2 were compared using a chi-square test. Progression-free survival and overall survival were analyzed by the Kaplan-Meier method, and p values were reported using the log-rank (Mantel-Cox) test.

Data and Software Accessibility

The accession number for the transcriptome data reported in this paper is ArrayExpress: E-MTAB-6488. The accession number for the targeted exome sequencing data reported in this paper is ArrayExpress: E-MTAB-6546. All original, unprocessed data can be accessed at Mendeley Data (https://doi.org/10.17632/jkm5vdz42z.1).

SUPPLEMENTAL INFORMATION

Supplemental Information includes Supplemental Experimental Procedures, seven figures, and six tables and can be found with this article online at https://doi.org/10.1016/j.celrep.2018.02.089.

ACKNOWLEDGMENTS

This work was supported by the Julians Stichting; an NWO-VIDI grant (91713334) to M.A.T.M.v.V.; a Dutch Cancer Society/KWF project grant (RUG 2014-7471) to W.F.A.d.D.; a Kinder Kankervrij (KiKa) grant (project 94) to S.L.A.P. and E.S.J.M.d.B.; a Stichting Kinderoncologie Groningen/SKOG project grant (16-02) to S.W.M.B., V.G., and E.S.J.M.d.B.; and a Dutch Cancer Society/KWF career award (RUG 2014-6903) to S.W.M.B. We thank Dr. Michael Schubert for advice on statistics. We apologize to all authors whose work we could not cite due to space restrictions.

AUTHOR CONTRIBUTIONS

Conceptualization, W.W.Z., S.L.A.P., E.S.J.M.d.B., and S.W.M.B.; Methodology, W.W.Z., S.L.A.P., E.S.J.M.d.B., S.W.M.B., V.G., D.O.W., F.F., A.v.d.B., and M.A.T.M.v.V.; Software and Formal Analysis, W.W.Z. and V.G.; Investigation, W.W.Z., F.J.S., T.G.J.M.-d.B., H.J.L., S.G.L., M.J.S., S.C., L.S.-M., A.S., and L.C.v.K.; Resources, W.W.Z., L.M., C.E.M.G., E.W.H., F.A.E.K., W.F.A.d.D., P.W., and E.H.; Data Curation, V.G.; Writing, W.W.Z. and S.W.M.B.; Writing – Review and Editing, W.W.Z., S.W.M.B., E.S.J.M.d.B., S.L.A.P., V.G., M.A.T.v.V., A.v.d.B., P.W., and F.F.; Visualization, W.W.Z.; Supervision and Project Administration, S.L.A.P., V.G., E.S.J.M.d.B., S.W.M.B.; Funding Acquisition, M.A.T.M.v.V., W.F.A.d.D., S.L.A.P., V.G., E.S.J.M.d.B., S.W.M.B.

DECLARATION OF INTERESTS

The authors declare no competing interests.

Received: October 19, 2017
Revised: January 8, 2018
Accepted: February 22, 2018
Published: March 20, 2018

REFERENCES

Aebersold, R., and Mann, M. (2016). Mass-spectrometric exploration of proteome structure and function. Nature *537*, 347–355.

Akbani, R., Ng, P.K.S., Werner, H.M.J., Shahmoradgoli, M., Zhang, F., Ju, Z., Liu, W., Yang, J.-Y., Yoshihara, K., Li, J., et al. (2014). A pan-cancer proteomic perspective on The Cancer Genome Atlas. Nat. Commun. *5*, 3887.

Akita, H., Marquardt, J.U., Durkin, M.E., Kitade, M., Seo, D., Conner, E.A., Andersen, J.B., Factor, V.M., and Thorgeirsson, S.S. (2014). MYC activates stem-like cell potential in hepatocarcinoma by a p53-dependent mechanism. Cancer Res. *74*, 5903–5913.

Anagnostopoulos, A.K., Papathanassiou, C., Karamolegou, K., Anastasiadou, E., Dimas, K.S., Kontos, H., Koutsopoulos, A., Prodromou, N., Tzortzatou-Stathopoulou, F., and Tsangaris, G.T. (2015). Proteomic studies of pediatric medulloblastoma tumors with 17p deletion. J. Proteome Res. *14*, 1076–1088.

Bien-Willner, G.A., and Mitra, R.D. (2014). Mutation and expression analysis in medulloblastoma yields prognostic variants and a putative mechanism of disease for i17q tumors. Acta Neuropathol. Commun. *2*, 74.

Cavalli, F.M.G., Remke, M., Rampasek, L., Peacock, J., Shih, D.J.H., Luu, B., Garzia, L., Torchia, J., Nor, C., Morrissy, A.S., et al. (2017). Intertumoral Heterogeneity within Medulloblastoma Subgroups. Cancer Cell *31*, 737–754.e6.

Cojoc, M., Mäbert, K., Muders, M.H., and Dubrovska, A. (2015). A role for cancer stem cells in therapy resistance: cellular and molecular mechanisms. Semin. Cancer Biol. *31*, 16–27.

Coller, H.A., Grandori, C., Tamayo, P., Colbert, T., Lander, E.S., Eisenman, R.N., and Golub, T.R. (2000). Expression analysis with oligonucleotide microarrays reveals that MYC regulates genes involved in growth, cell cycle, signaling, and adhesion. Proc. Natl. Acad. Sci. USA *97*, 3260–3265.

Conroy, S., Kruyt, F.A.E., Joseph, J.V., Balasubramaniyan, V., Bhat, K.P., Wagemakers, M., Enting, R.H., Walenkamp, A.M.E., and den Dunnen, W.F.A. (2014). Subclassification of newly diagnosed glioblastomas through an immunohistochemical approach. PLoS ONE *9*, e115687.

Dang, C.V. (2012). MYC on the path to cancer. Cell *149*, 22–35.

de Bono, J.S., and Ashworth, A. (2010). Translating cancer research into targeted therapeutics. Nature *467*, 543–549.

Downing, J.R., Wilson, R.K., Zhang, J., Mardis, E.R., Pui, C.-H., Ding, L., Ley, T.J., and Evans, W.E. (2012). The Pediatric Cancer Genome Project. Nat. Genet. *44*, 619–622.

Fagnocchi, L., and Zippo, A. (2017). Multiple Roles of MYC in Integrating Regulatory Networks of Pluripotent Stem Cells. Front. Cell Dev. Biol. *5*, 7.

Galardi, S., Savino, M., Scagnoli, F., Pellegatta, S., Pisati, F., Zambelli, F., Illi, B., Annibali, D., Beji, S., Orecchini, E., et al. (2016). Resetting cancer stem cell regulatory nodes upon MYC inhibition. EMBO Rep. *17*, 1872–1889.

Hanahan, D. (2014). Rethinking the war on cancer. Lancet *383*, 558–563.

Hanahan, D., and Weinberg, R.A. (2011). Hallmarks of cancer: the next generation. Cell *144*, 646–674.

Harris, P.S., Venkataraman, S., Alimova, I., Birks, D.K., Balakrishnan, I., Cristiano, B., Donson, A.M., Dubuc, A.M., Taylor, M.D., Foreman, N.K., et al. (2014). Integrated genomic analysis identifies the mitotic checkpoint kinase WEE1 as a novel therapeutic target in medulloblastoma. Mol. Cancer *13*, 72.

Hassan, H., Pinches, A., Picton, S.V., and Phillips, R.S. (2017). Survival rates and prognostic predictors of high grade brain stem gliomas in childhood: a systematic review and meta-analysis. J. Neurooncol. *135*, 13–20.

Hill, R.M., Kuijper, S., Lindsey, J.C., Petrie, K., Schwalbe, E.C., Barker, K., Boult, J.K.R., Williamson, D., Ahmad, Z., Hallsworth, A., et al. (2015). Combined MYC and P53 defects emerge at medulloblastoma relapse and define rapidly progressive, therapeutically targetable disease. Cancer Cell *27*, 72–84.

Jung, M., Russell, A.J., Liu, B., George, J., Liu, P.Y., Liu, T., DeFazio, A., Bowtell, D.D.L., Oberthuer, A., London, W.B., et al. (2017). A Myc activity signature predicts poor clinical outcomes in Myc-associated cancers. Cancer Res. *77*, 971–981.

Kawauchi, D., Robinson, G., Uziel, T., Gibson, P., Rehg, J., Gao, C., Finkelstein, D., Qu, C., Pounds, S., Ellison, D.W., et al. (2012). A mouse model of the most aggressive subgroup of human medulloblastoma. Cancer Cell *21*, 168–180.

Kim, J., Woo, A.J., Chu, J., Snow, J.W., Fujiwara, Y., Kim, C.G., Cantor, A.B., and Orkin, S.H. (2010). A Myc network accounts for similarities between embryonic stem and cancer cell transcription programs. Cell *143*, 313–324.

Kool, M., Koster, J., Bunt, J., Hasselt, N.E., Lakeman, A., van Sluis, P., Troost, D., Meeteren, N.S., Caron, H.N., Cloos, J., et al. (2008). Integrated genomics identifies five medulloblastoma subtypes with distinct genetic profiles, pathway signatures and clinicopathological features. PLoS ONE *3*, e3088.

Künkele, A., De Preter, K., Heukamp, L., Thor, T., Pajtler, K.W., Hartmann, W., Mittelbronn, M., Grotzer, M.A., Deubzer, H.E., Speleman, F., et al. (2012). Pharmacological activation of the p53 pathway by nutlin-3 exerts anti-tumoral effects in medulloblastomas. Neuro-oncol. *14*, 859–869.

Leon, J., Ferrandiz, N., Acosta, J.C., and Delgado, M.D. (2009). Inhibition of cell differentiation: a critical mechanism for MYC-mediated carcinogenesis? Cell Cycle *8*, 1148–1157.

Levine, A.J. (1997). p53, the cellular gatekeeper for growth and division. Cell *88*, 323–331.

Louis, D.N., Perry, A., Reifenberger, G., von Deimling, A., Figarella-Branger, D., Cavenee, W.K., Ohgaki, H., Wiestler, O.D., Kleihues, P., and Ellison, D.W. (2016). The 2016 World Health Organization Classification of Tumors of the Central Nervous System: a summary. Acta Neuropathol. *131*, 803–820.

Morrissy, A.S., Garzia, L., Shih, D.J., Zuyderduyn, S., Huang, X., Skowron, P., Remke, M., Cavalli, F.M., Ramaswamy, V., Lindsay, P.E., et al. (2016). Divergent clonal selection dominates medulloblastoma at recurrence. Nature *529*, 351–357.

Northcott, P.A., Jones, D.T.W., Kool, M., Robinson, G.W., Gilbertson, R.J., Cho, Y.-J., Pomeroy, S.L., Korshunov, A., Lichter, P., Taylor, M.D., and Pfister, S.M. (2012). Medulloblastomics: the end of the beginning. Nat. Rev. Cancer *12*, 818–834.

Northcott, P.A., Buchhalter, I., Morrissy, A.S., Hovestadt, V., Weischenfeldt, J., Ehrenberger, T., Gröbner, S., Segura-Wang, M., Zichner, T., Rudneva, V.A., et al. (2017). The whole-genome landscape of medulloblastoma subtypes. Nature *547*, 311–317.

Pei, Y., Moore, C.E., Wang, J., Tewari, A.K., Eroshkin, A., Cho, Y.J., Witt, H., Korshunov, A., Read, T.A., Sun, J.L., et al. (2012). An animal model of MYC-driven medulloblastoma. Cancer Cell *21*, 155–167.

Pui, C.H., Gajjar, A.J., Kane, J.R., Qaddoumi, I.A., and Pappo, A.S. (2011). Challenging issues in pediatric oncology. Nat. Rev. Clin. Oncol. *8*, 540–549.

Ramaswamy, V., Remke, M., Bouffet, E., Faria, C.C., Perreault, S., Cho, Y.J., Shih, D.J., Luu, B., Dubuc, A.M., Northcott, P.A., et al. (2013). Recurrence patterns across medulloblastoma subgroups: an integrated clinical and molecular analysis. Lancet Oncol. *14*, 1200–1207.

Ramaswamy, V., Remke, M., Bouffet, E., Bailey, S., Clifford, S.C., Doz, F., Kool, M., Dufour, C., Vassal, G., Milde, T., et al. (2016). Risk stratification of childhood medulloblastoma in the molecular era: the current consensus. Acta Neuropathol. *131*, 821–831.

Roussel, M.F., and Robinson, G.W. (2013). Role of MYC in Medulloblastoma. Cold Spring Harb. Perspect. Med. *3*, a014308.

Schoppy, D.W., Ragland, R.L., Gilad, O., Shastri, N., Peters, A.A., Murga, M., Fernandez-Capetillo, O., Diehl, J.A., and Brown, E.J. (2012). Oncogenic stress sensitizes murine cancers to hypomorphic suppression of ATR. J. Clin. Invest. *122*, 241–252.

Sharma, K., D'Souza, R.C.J., Tyanova, S., Schaab, C., Wiśniewski, J.R., Cox, J., and Mann, M. (2014). Ultradeep human phosphoproteome reveals a distinct regulatory nature of Tyr and Ser/Thr-based signaling. Cell Rep. *8*, 1583–1594.

Soucek, L., Whitfield, J.R., Sodir, N.M., Massó-Vallés, D., Serrano, E., Karnezis, A.N., Swigart, L.B., and Evan, G.I. (2013). Inhibition of Myc family proteins eradicates KRas-driven lung cancer in mice. Genes Dev. *27*, 504–513.

Spiegler, B.J., Bouffet, E., Greenberg, M.L., Rutka, J.T., and Mabbott, D.J. (2004). Change in neurocognitive functioning after treatment with cranial radiation in childhood. J. Clin. Oncol. *22*, 706–713.

Staal, J.A., Lau, L.S., Zhang, H., Ingram, W.J., Hallahan, A.R., Northcott, P.A., Pfister, S.M., Wechsler-Reya, R.J., Rusert, J.M., Taylor, M.D., et al. (2015). Proteomic profiling of high risk medulloblastoma reveals functional biology. Oncotarget *6*, 14584–14595.

Taylor, M.D., Northcott, P.A., Korshunov, A., Remke, M., Cho, Y.-J., Clifford, S.C., Eberhart, C.G., Parsons, D.W., Rutkowski, S., Gajjar, A., et al. (2012). Molecular subgroups of medulloblastoma: the current consensus. Acta Neuropathol. *123*, 465–472.

Truitt, M.L., and Ruggero, D. (2016). New frontiers in translational control of the cancer genome. Nat. Rev. Cancer *16*, 288–304.

Valentijn, L.J., Koster, J., Haneveld, F., Aissa, R.A., van Sluis, P., Broekmans, M.E.C., Molenaar, J.J., van Nes, J., and Versteeg, R. (2012). Functional MYCN signature predicts outcome of neuroblastoma irrespective of MYCN amplification. Proc. Natl. Acad. Sci. USA *109*, 19190–19195.

van Riggelen, J., Yetil, A., and Felsher, D.W. (2010). MYC as a regulator of ribosome biogenesis and protein synthesis. Nat. Rev. Cancer *10*, 301–309.

Wang, W.J., Wu, S.P., Liu, J.B., Shi, Y.S., Huang, X., Zhang, Q.B., and Yao, K.T. (2013). MYC regulation of CHK1 and CHK2 promotes radioresistance in a stem cell-like population of nasopharyngeal carcinoma cells. Cancer Res. *73*, 1219–1231.

Wang, X., Dubuc, A.M., Ramaswamy, V., Mack, S., Gendoo, D.M.A., Remke, M., Wu, X., Garzia, L., Luu, B., Cavalli, F., et al. (2015). Medulloblastoma subgroups remain stable across primary and metastatic compartments. Acta Neuropathol. *129*, 449–457.

Whitfield, J.R., Beaulieu, M.-E., and Soucek, L. (2017). Strategies to Inhibit Myc and Their Clinical Applicability. Front. Cell Dev. Biol. *5*, 10.